Available online at www.sciencedirect.com
ScienceDirect
Construction and Building Materials 22 (2008) 186–199
Construction and Building MATERIALS
www.elsevier.com/locate/conbuildmat

Longterm corrosion performance of rebar embedded in blended cement concrete under macro cell corrosion condition

R. Vedalakshmi [a,*], K. Rajagopal [b], N. Palaniswamy [a]

[a] Corrosion Protection Division, Central Electrochemical Research Institute, Karaikudi, TamilNadu 630 006, India
[b] Department of Civil Engineering, A.C. College of Engineering and Technology, Karaikudi, Tamil Nadu 630 004, India

Received 7 September 2006; accepted 8 September 2006
Available online 22 November 2006

Abstract

The concrete does not possess sufficient resistance towards the permeation of aggressive ions when it is exposed to marine environment. When mineral admixtures are added, they impart certain impermeability to concrete by improving the physical structure by pozzolanic reaction. The reduction of concentration of OH^- ion occurs either by consumption of free $Ca(OH)_2$ by pozzolanic reaction or by dilution of cement alkalis due to replacement with mineral admixture. This causes a substantial reduction in the threshold value of chloride in mineral admixed concrete. In the present investigation, the corrosion resistance of rebar embedded in concrete made with Portland pozzolana cement (PPC), Portland slag cement (PSC) was studied for 847 days under macro cell corrosion condition with on comparison using ordinary Portland cement (OPC). Concrete having characteristic compressive strength of 20, 30 and 40 MPa were taken for evaluation. Potential and macro cell corrosion current were measured periodically and corrosion rates were determined by weight-loss method. This long term experiment revealed that in 20 MPa concrete, the corrosion rate of rebar in PPC and PSC concrete was 9 and 10 times lower than the rebar in OPC concrete: In the case of 30 MPa concrete, the corrosion rate of rebar in PPC and PSC concrete was 17 and 6 times lower respectively and in 40 MPa concrete it was 1.6–2.5 times less than the rebar in OPC concrete. The reduction of chloride ion content in blended cement concrete was varied from 1.4 to 3.1 times less than the OPC concrete among all the three concretes studied. Reduction of alkalinity in 20 MPa concrete at the rebar level in PPC and PSC concrete is 6 and 10 times lower, respectively, than in OPC concrete. In the case of 30 and 40 MPa concrete it was 2 and 1.6 times lower. The reduction in alkalinity did not accelerate the corrosion rate of rebar in blended cement concretes even in presence of higher amount of chlorides. The apparent chloride diffusion co-efficient of blended cement concretes was 1.6–1.8 times lower than that of OPC concrete. The combined effect of higher chloride complexing ability and reduction of chloride ion diffusivity of blended cement concretes made them to perform better in terms of corrosion protection of reinforcing steel.

Keywords: Blended cements; Macro cell corrosion; Corrosion rate; Chloride diffusion co-efficient; Pozzolanic reaction

1. Introduction

Corrosion of rebar embedded in concrete is one of the foremost factors that affect the durability of concrete structures in marine environments. The chloride ions depassivate the steel and cause dissolution of the metal at the location called 'anode' or 'active zone'. This active zone is surrounded by a 'passive zone' called 'cathode' where oxygen reduction takes place [1]. The cell constituting separate anodic and cathodic regions is termed as 'macro cell'. This creates relatively large-scale potential gradients between anode and cathode causing flow of corrosion current [2]. These cells are more prevalent in chloride-contaminated concrete with a spatial separation of 100 mm or more between anodes and cathodes in the same rebar [3]. To simulate marine substructure condition in the laboratory, studies were made on by forming chloride ion concentration gradient in concrete, which accelerated the

* Corresponding author. Tel.: +91 4565 227550; fax: +91 4565 227113.
E-mail address: corrveda@yahoo.co.in (R. Vedalakshmi).

0950-0618/$ - see front matter © 2006 Elsevier Ltd. All rights reserved.
doi:10.1016/j.conbuildmat.2006.09.004

corrosion. The formation of macro corrosion cells in marine environment caused the localized pitting in the region of crack [4]. Studies were made on the effect of w/c ratio, cover depth and area of anode to cathode ratio during corrosion propagation under macro cell corrosion condition [5] and it was found that the rate of corrosion on the anode mainly depended on chloride content and oxygen supply. The effect of active and passive area of rebar under macro cell corrosion condition was studied by embedding the face-to-face electrodes and coplanar electrodes in concrete [6]. The corrosion rate of rebar was a function of the difference in potential, ohmic resistance of the concrete and polarization resistance of the rebar. The effect of damages on the performance of various coatings such as fusion bonded epoxy coating, inhibited cement slurry coating and galvanizing was investigated using accelerated macrocell corrosion test [7–9]. In actual field, long term corrosion monitoring of concrete structures had also been attempted by creating macro cell corrosion condition either by embedding the stainless steel electrodes or by embedding the steel in high chloride concrete [10]. ASTM [11] also evolved a standard for this type of macro cell corrosion studies to evaluate the chemical admixtures in chloride-contaminated concrete. The specimen configuration as specified in ASTM G109 earlier has been modified by incorporating two separate reinforcement triads (one bar at top and two bars at bottom) into a single concrete specimen to reduce the batch variation for evaluating the different types of corrosion inhibiting admixture [12]. The corrosion efficiency of organic chelatin-based admixtures in concrete was studied using ASTM G109 specifications but under cracked condition [13]. By loading the specimens, the cracks were induced in the middle of the beam to a depth up to the top of the bar and macro cell current was measured.

The impermeability of concrete is improved by adding mineral admixtures during mixing of the concrete [14–17]. In blended cements, the mineral admixtures are added by inter-grinding along with clinker and gypsum in the cement mill. There is a difference in the behaviour of such blended cements. It was reported that the concrete made with the inter-grinding blended cements gain strength more rapidly than the mineral admixtures added at site [18]. The use of low w/c ratio concretes made with blended cements under controlled curing were most likely to ensure optimal performance of concrete in terms of corrosion of steel under high chloride conditions [19,20]. The studies conducted on slag cement paste concluded that the presence of redox species such as S^-, HS^- and S^{n-} in slag reduced the passivity of the rebar [21]. In spite of the reduction in OH^- concentration in fly ash and slag added concrete, the corrosion rate of rebar remained unaffected [15,19]. Uncertainties in earlier reports necessitated a detailed investigation on corrosion performance of rebar embedded in blended cement concretes.

In this study ordinary Portland cement was replaced with 25% of fly ash and 50% slag. To accelerate the corrosion, macro cell corrosion condition was created by forming chloride ion concentration gradient in concrete. The performance was compared with the concrete made with ordinary Portland cement (OPC).

2. Experimental

2.1. Materials and mix proportions

Three mix proportions having characteristic compressive strength of 20, 30 and 40 MPa concrete at 28 days were used for casting the concrete specimens. The details of mix proportions are given in Table 1. The cement content and w/c ratio were kept constant for both blended cement concretes and Portland cement concrete. Three cements namely 43 grade ordinary Portland cement conforming to I.S:81129 ([22] equivalent to ASTM – Type-I cement), Portland pozzolana cement conforming to I.S.1489 – Part-I [23] and Portland slag cement conforming to I.S:455 [24] were used. Chemical composition of cements used as given by the manufacturer is reproduced and given in Table 2. Well graded river sand and good quality crushed blue granite were used as fine and coarse aggregates respectively. The different size fractions of coarse aggregate (20 mm down graded and 12.5 mm down graded) were taken and recombined to a specified grading as shown in Table 3. Sixteen millimeter diameter cold twisted high yield strength deformed bar (Fe-415 grade) conforming to I.S.1786 [25] was used and its chemical com-

Table 1
Detail of concrete mix proportions

Grade	Type of cement	w/c Ratio	Cement (Kg/m^3)	Water (Kg/m^3)	Fine aggregate (Kg/m^3)	Coarse aggregate (Kg/m^3)
M20	OPC	0.67	284	190	770	1026
	PPC	0.67	284	190	770	1026
	PSC	0.67	284	190	770	1026
M30	OPC	0.54	352	190	739	1026
	PPC	0.54	352	190	739	1026
	PSC	0.54	352	190	739	1026
M40	OPC	0.42	452	190	655	1026
	PPC	0.42	452	190	655	1026
	PSC	0.42	452	190	655	1026

Table 2
Chemical composition of three types of cement

Compound	Ordinary Portland Cement (%)	Portland Pozzolana cement (%)	Portland slag cement (%)
Silicon-di-oxide (SiO_2)	20–21	28–32	26–30
Aluminium oxide (Al_2O_3)	5.2–5.6	7.0–10.0	9.0–11.0
Ferric oxide (Fe_2O_3)	4.4–4.8	4.9–6.0	2.5–3.0
Calcium oxide (CaO)	62–63	41–43	44–46
Magnesium oxide (MgO)	0.5–0.7	1.0–2.0	3.5–4.0
Sulphur-tri-oxide (SO_3)	2.4–2.8	2.4–2.8	2.4–2.8
Loss on ignition	1.5–2.5	3.0–3.5	1.5–2.5
Bogue compound composition			
Tricalcium silicate (C_3S)	42–45	Not applicable	Not applicable
Dicalcium silicate (C_2S)	20–30	-do-	-do-
Tricalcium aluminate (C_3A)	7.0-9.0	-do-	-do-
Tetra calcium alumino ferrite (C_4AF)	11–13	-do-	-do-
Physical properties			
Pozzalanic material used (%)	–	Around 20% flyash (Mettur Thermal power station)	Around 50% GGBS (Vizag Steel plant)
28 Day compressive strength (MPa)	62	48	53
Fineness (m^2/kg)	295	363	385

Table 3
Grading of coarse and fine aggregate

Coarse aggregate		Fine aggregate	
Sieve size (mm)	Cumulative % retained	Sieve size (mm)	Cumulative % retained
20	0	4.75	0
16	25	2.36	12
12.5	52	0.600	49
10	72	0.300	85
4.75	100	0.150	97
		<0.150	100

position is C-0.17%; Mn-0.66%; Si-0.115; S-0.017%; P-0.031 and Fe-Balance. Potable water was used for casting the concrete.

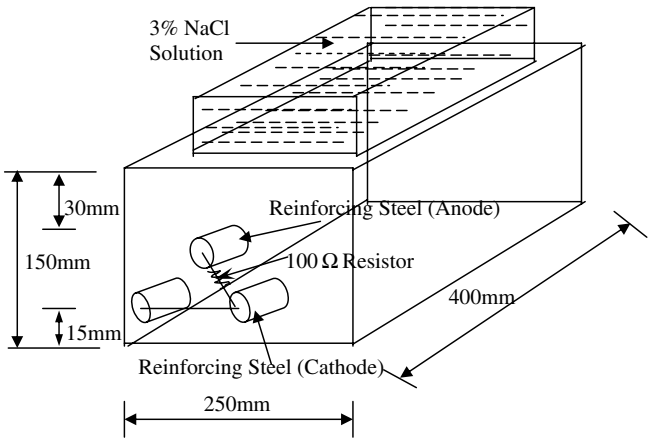

Fig. 1a. Modified ASTM G109-94a corrosion test prism.

2.2. Specimen details

Concrete specimen of size 400 × 250 × 150 mm as shown in Fig. 1a was used. In each specimen, a 16 mm dia bar of 320 mm length was embedded at 30 mm cover from the top. Two rebars having 450 mm length were embedded at 15 mm cover from the bottom. While embedding these bars at bottom, they were kept in such a way that 80 mm lengths of these bars were protruded outside of the concrete specimen. Before embedding, the rust scale was removed from all the bars by chemical cleaning in inhibited hydrochloric acid and then dried. Initial weight of the top rebar was measured. After measuring the initial weight, the stem of size 6 mm dia and 100 mm length was screwed on the top of the rebar as shown in Fig. 1b and from this electrical leads were taken. This facilitates the top rebar fully kept inside the concrete and will not be exposed to outside. By means of this at the end of the exposure, after removing the stem the final weight of the top rebar could be made accurately. Duplicate specimens were cast. After demoulding, the specimens were cured for 28 days. After curing, electrical leads were taken from all the three bars. The rod protruding outside the specimen was sealed by using epoxy compound in order to eliminate the crevice corrosion at these locations. A bund of 345 × 195 × 13 mm size was constructed on the top of the each specimen using 1:1 cement mortar and was sealed in all sides using epoxy resin. As shown in Fig. 2 all the specimens were taken to the exposure yard and kept on the concrete specimens thus allowing free air flow under the specimens.

2.3. Method of exposure

The specimens were subjected to alternate wetting in 3% NaCl solution and drying test. Three per cent NaCl solu-

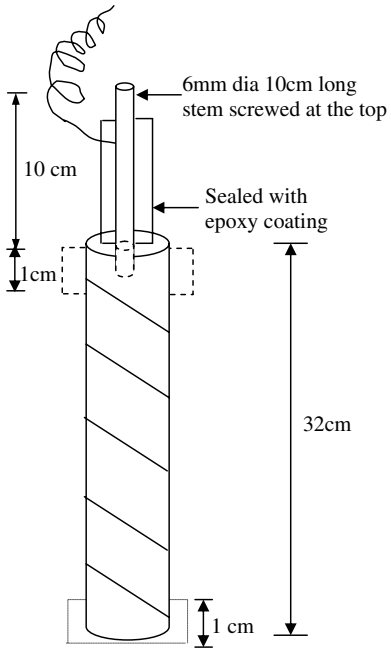

Fig. 1b. Rebar end and protection details.

tion was ponded over the top of each for 4 days and allowed to dry for 3 days and thus 7 days constituted one cycle of alternate wetting and drying. During exposure to salt solution, chloride ions tend to diffuse through the cover concrete and cause corrosion of the top rebar. During the entire exposure period, the chloride concentration is higher at the top of the specimen when compared to the bottom of the specimen and thus creates a chloride ion concentration gradient. Because of high chloride at top, the top rebar acts as an anode and bottom bars act as cathode. The area of the anode to cathode ratio was kept as 1:2 to accelerate the corrosion process. The experiment was conducted over a period of 847 days.

2.4. Method of measurement

The initial half-cell potential measurements were made on the top rebar using high input impedance multimeter. Saturated calomel electrode was used as the reference electrode. Then all the rebars were electrically short-circuited. The galvanic current also called macro cell current flow between top and bottom bars was measured once in a month at the end of wet cycle as per procedures outlined in ASTM G109-94a [11]. A 100-ohm resistor was placed between the top and bottom rebars and the potential difference was measured. The current was calculated from this as:

$$I_c = V \div R, \quad \text{where } R = 100 \text{ ohms} \tag{1}$$

The increase in anodic current indicates the initiation of corrosion. After measuring the current, at the end of each cycle, the half-cell potential of the top rebar was measured for each specimen after 1 h thus allowing depolarization of rebar to reach the steady state. The potential-time behaviour of rebar embedded in three concretes are compared and given in Figs. 3–5. Similarly in Figs. 6–8 the change in macro cell current with time was compared.

At the end of the exposure period, the specimens were broken open and both the top and bottom rebars were taken out and examined visually. The extent of rust on the top rebar in 20, 30 and 40 MPa concrete is shown in Figs. 9–11, respectively.

2.5. Corrosion rate from gravimetric weight-loss

The stem was removed from top rebar in all the specimens. After pickling the rebars in inhibited hydrochloric acid as specified in ASTM G1 [26], the final weight was measured. From the initial and final weight, the corrosion rate in mmpy was calculated using the following formulae:

Fig. 2. Concrete specimens under exposure conditions in exposure yard.

$$\text{Corrosion rate in mmpy} = \frac{87.6 \times w}{DAT} \quad (2)$$

where w is the loss in weight, mg; D the Density of Iron, g/cm^3; A the Area, cm^2; and T is the Time, h.

The results are given in Fig. 12.

2.6. Determination of Cl^- and OH^- ion concentration

2.6.1. OH^- ions concentration

The concentration of OH^- ions was determined from the powdered concrete sample by decantation method. As reported [27] though this method overestimates the OH^- ion concentration, this has been carried out for relative comparison of concretes having different w/c ratio and cement content. For this, the concrete core samples up to a depth of 120 mm were taken from one of the duplicate specimens. Then the sample was sliced at every 30 mm depth up to a depth of 90 mm. Each slice was powdered and sieved through a 600 μm sieve. Then this powder was mixed with distilled water at the ratio of 1:3 by weight, respectively. This mixture was taken in a closed glass tube and shaken for 10 min and kept for 48 h. After 48 h, the solution was filtered and this solution was used to determine the OH^- ion concentration. A known amount of solution was titrated against 0.1 N H_2SO_4 using phenolpthalin as an indicator and from the titrated value, the OH^- ion concentration was calculated. The results are given in Table 4.

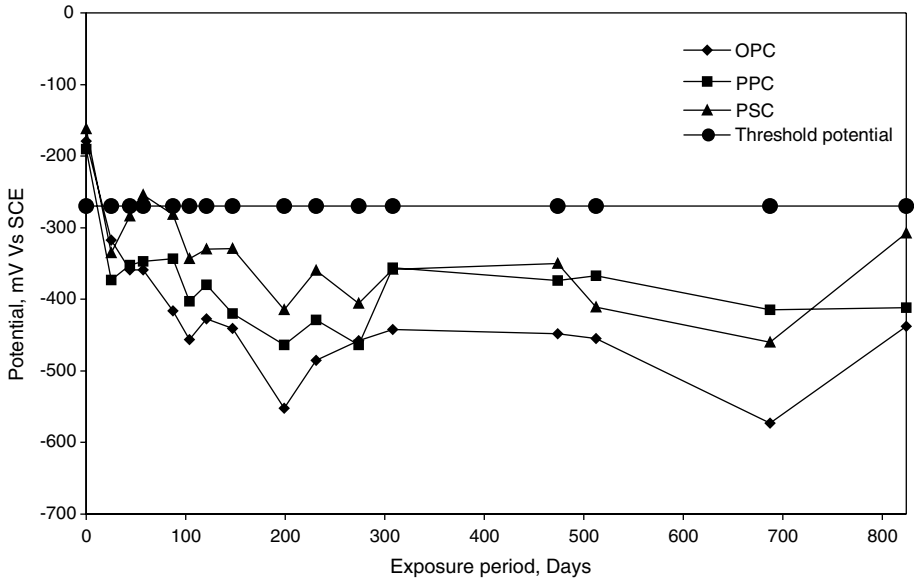

Fig. 3. Potential-time behaviour of rebar embedded in 20 MPa concrete.

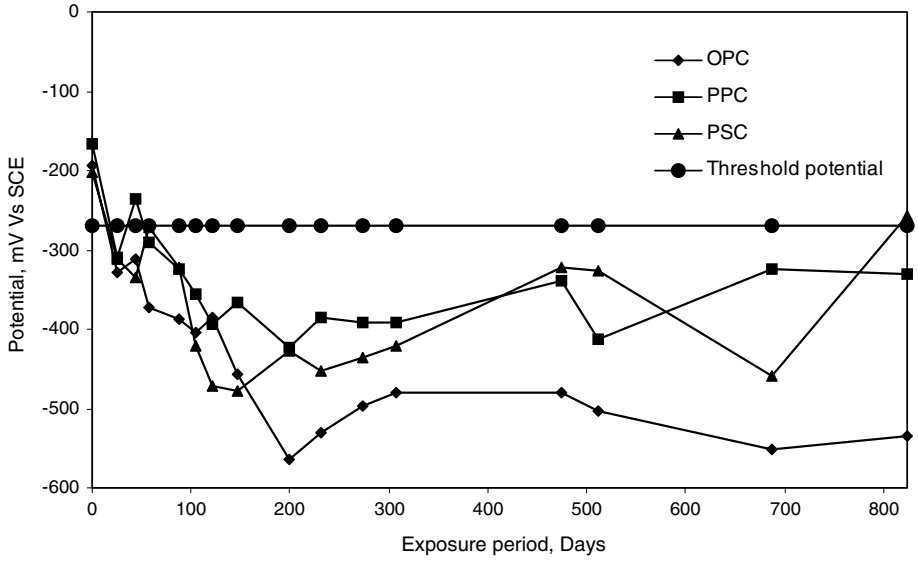

Fig. 4. Potential-time behaviour of rebar embedded in 30 MPa concrete.

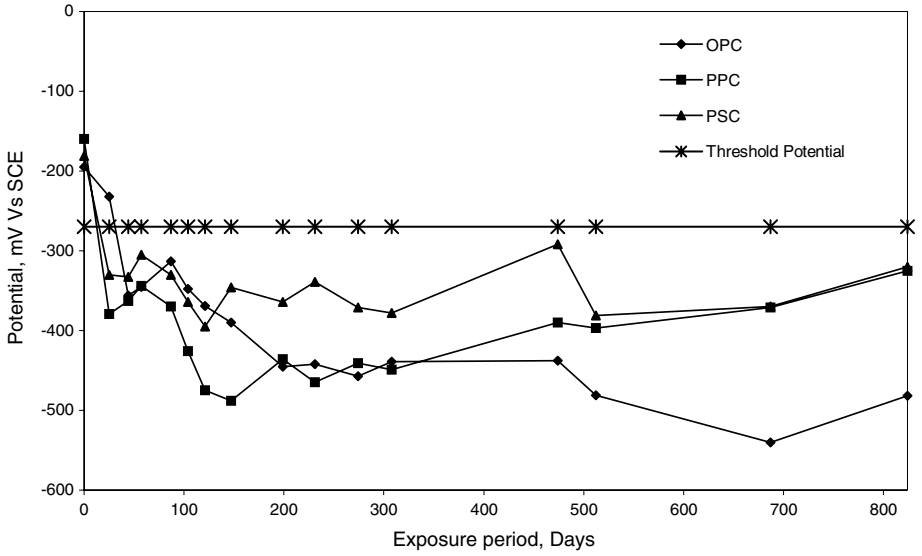

Fig. 5. Potential-time behaviour of rebar embedded in 40 MPa concrete.

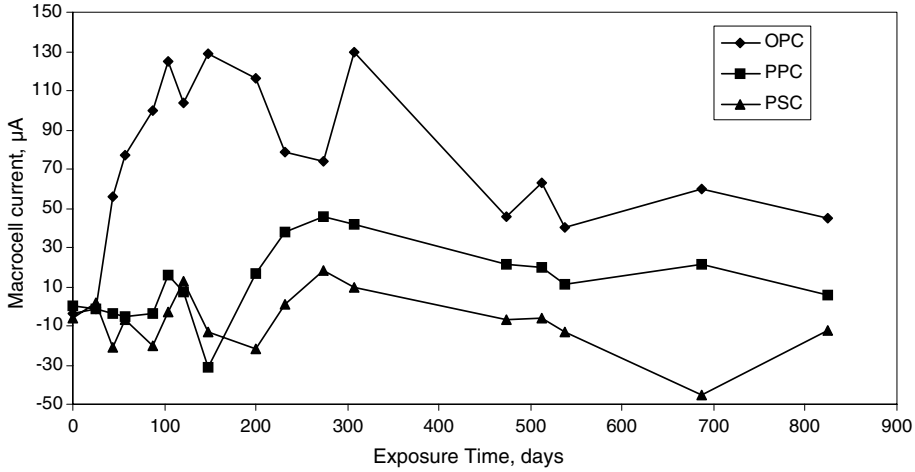

Fig. 6. Variation of macro cell current with time of rebar embedded in 20 MPa concrete.

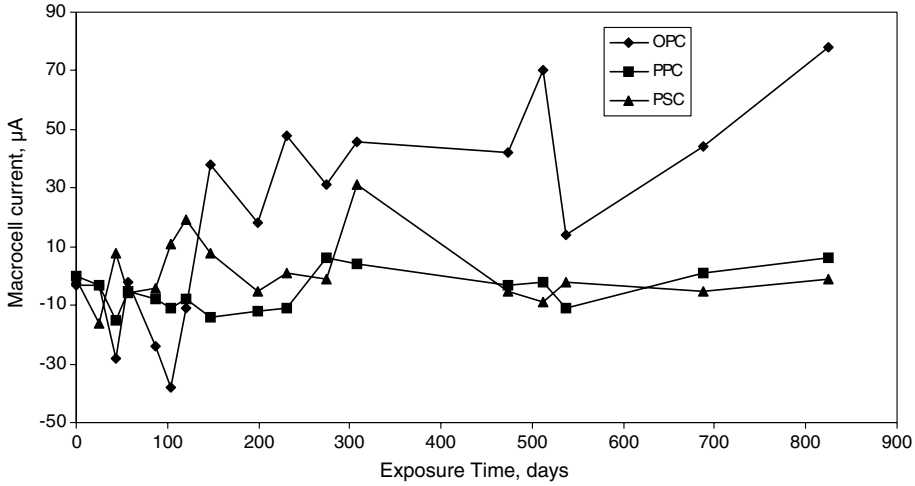

Fig. 7. Variation of macro cell current with time of rebar embedded in 30 MPa concrete.

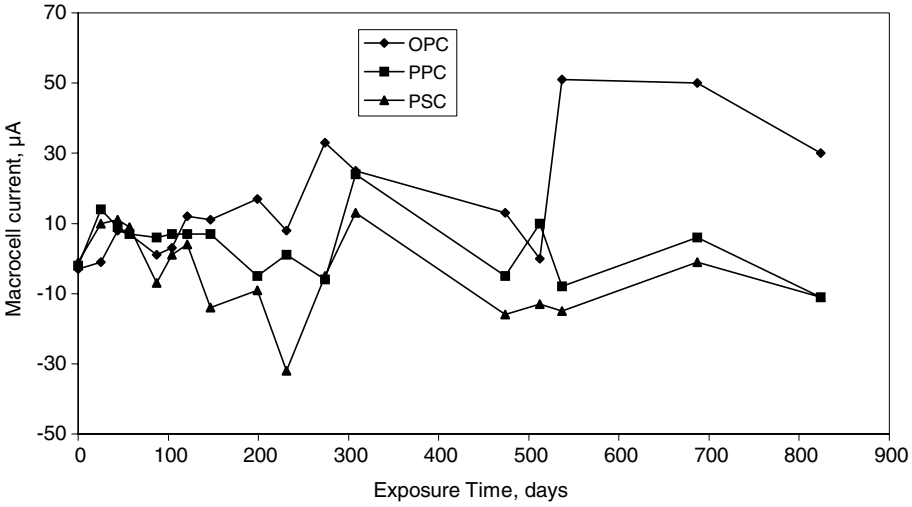

Fig. 8. Variation of macro cell current with time of rebar embedded in 40 MPa concrete.

2.6.2. Cl^- ions concentration

When chloride ions diffuse through the concrete some of the ions react with the hydration products and form calcium chloroaluminate and some chloride ions are adsorbed to the various hydrates of cement. A portion of chloride ions that remains free is termed as free chloride and this will cause corrosion of rebar [28]. Free Cl^- ions can be determined from the pore solution. The water soluble chloride (using water as an extraction medium) from the powdered concrete sample offer a more practical method than the pore extraction method since in the latter method, if the specimen is dry it becomes almost impossible to extract any solution [29]. In addition to this, the water soluble chloride is independent of the method of extraction, if the extraction period is greater than 24 h [30].

In the present study, the water-soluble chloride content was determined by volumetric analysis using the silver nitrate method [31,32]. The decanted solution filtered for OH^- ion concentration was used for chloride determination also. Five millilitre of solution was titrated against 0.01 N silver nitrate using potassium chromate as an indicator. From the titrated value, the Cl^- ion concentration was calculated and the results are given in Table 4.

2.7. Determination of diffusion co-efficient of chloride

The chloride ion diffusion coefficient can be calculated if the chloride concentration at the concrete surface as well as chloride concentration at any known depth are known. Fick's second law of diffusion is frequently used for this

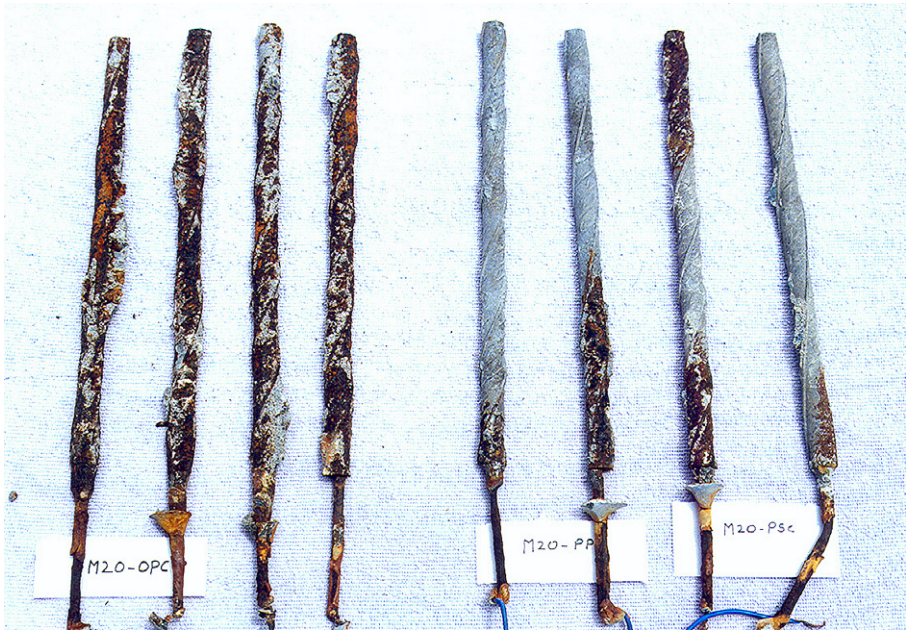

Fig. 9. Extent of rust of on rebars embedded in 20 MPa concrete.

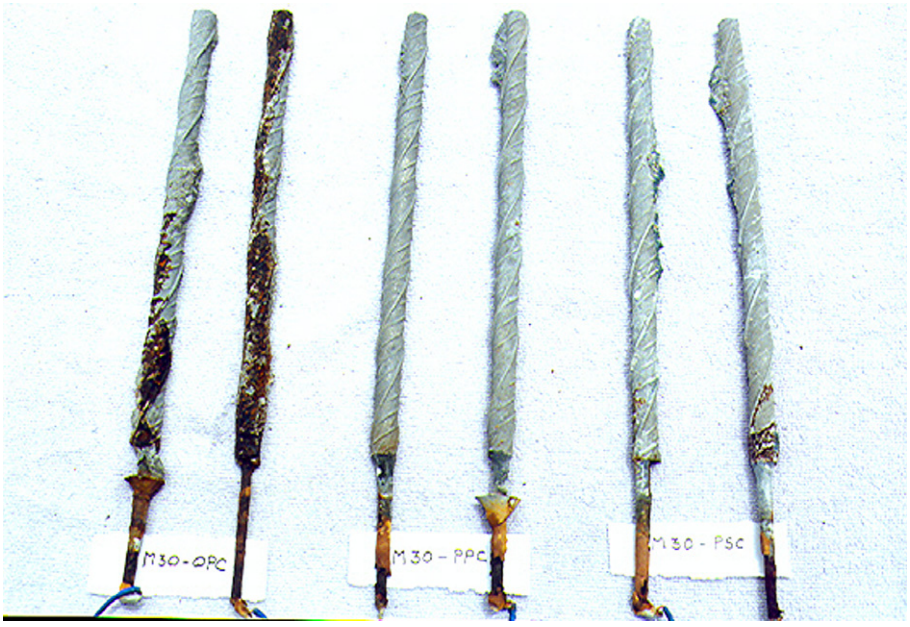

Fig. 10. Extent of rust on rebars embedded in 30 MPa concrete.

purpose where chloride ion diffusion into the concrete is from one direction only [33]

$$\frac{\partial c}{\partial t} = D_a \frac{\partial^2 c}{\partial x^2} \tag{3}$$

An analytical solution to Eq. (3), assuming that the flux of chlorides at any time is proportional to the chloride concentration gradient in the concrete of a semi-infinite medium is as follows [34]:

$$C_x = C_s \left[1 - \text{erf}\left(\frac{x}{2\sqrt{D_a t}}\right)\right] \tag{4}$$

where C_x is the chloride ion concentration at depth x , mol/l; x the thickness of concrete, cm; t the exposure time, s; C_s the surface chloride concentration at the concrete surface, mol/l; D_a the apparent chloride diffusion co-efficient, cm^2/s; and erf is the gaussian error function.

The error function from the standard mathematical tables [35] was used. Using Eq. (4), from the chloride concentration determined at various depths (C_x) and taking 3% NaCl (ponding solution) as the surface chloride concentration (C_s), the D_a was calculated for different depth and the average value was reported (Fig. 13).

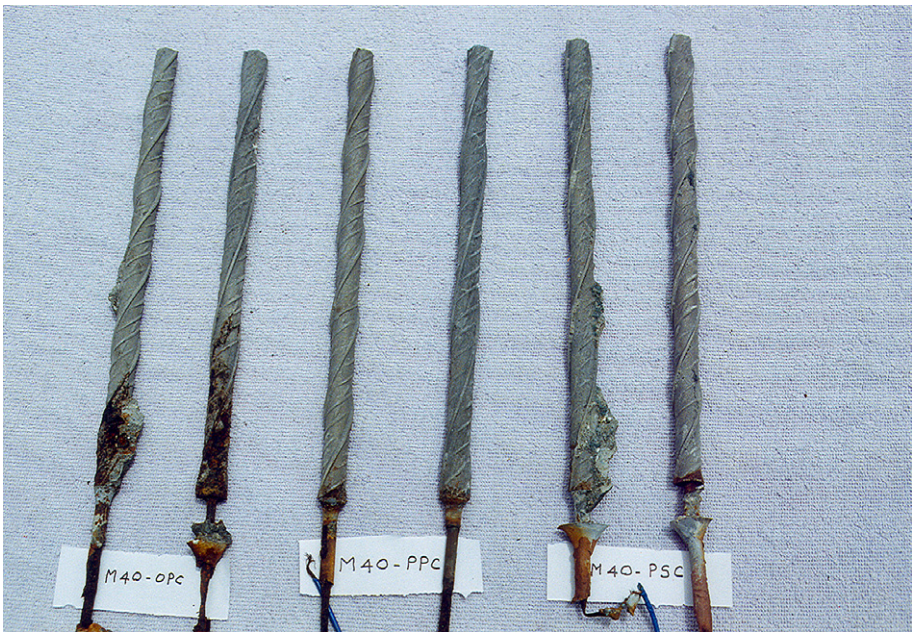

Fig. 11. Extent of rust on rebars embedded in 40 MPa concrete.

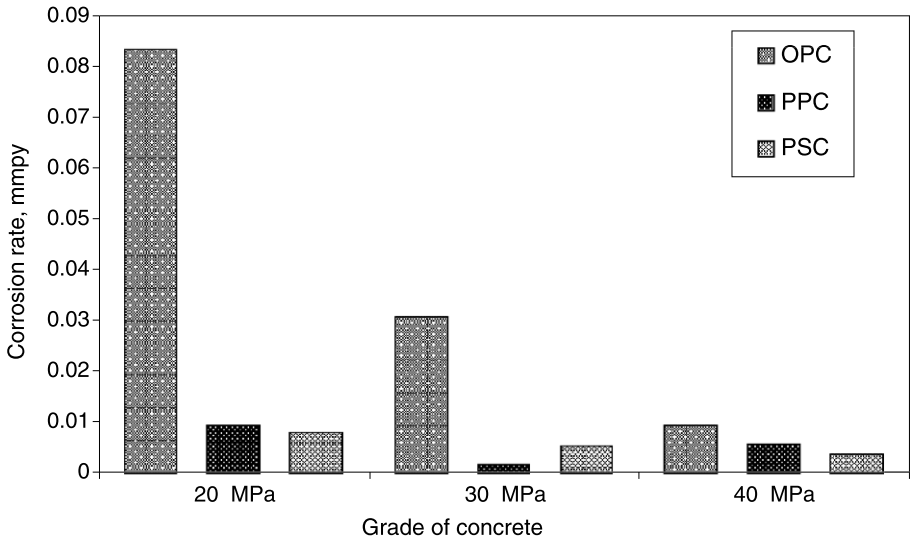

Fig. 12. Comparison of corrosion rate at the end of 847 days of exposure.

Table 4
Comparison of Cl^- and OH^- ion concentration of three concretes at various depths

Grade of concrete	Type of cement	Cl^- ion concentration in various depth (mm)						OH^- ion concentration (ppm)		
		ppm			% by weight of cement			Depth (mm)		
		0–30	30–60	60–90	0–30	30–60	60–90	0–30	30–60	60–90
M20	OPC	8946	8307	7455	7.12	6.59	5.92	2040	2244	2142
	PPC	10011	5751	5751	7.94	4.56	4.56	204	204	621
	PSC	7455	4686	4899	5.92	3.72	3.89	204	194	406
M30	OPC	10437	7668	8094	6.7	4.93	5.21	2040	2141	2244
	PPC	5964	5325	3408	3.84	3.42	2.19	510	1020	1020
	PSC	5325	5325	3834	3.42	3.42	2.47	235	1020	918
M40	OPC	8946	7881	7242	4.47	3.95	3.63	1887	2244	2142
	PPC	5325	2982	3195	2.67	1.49	1.60	551	1387	1122
	PSC	4473	2556	2343	2.24	1.28	1.17	1020	1428	1326

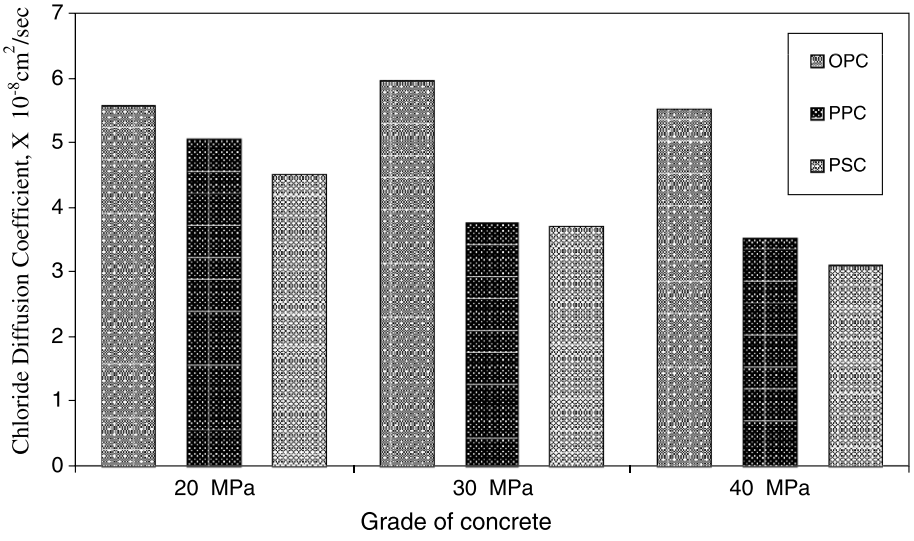

Fig. 13. Comparison of "D_a" value at the end of 847 days of exposure.

3. Results

3.1. Potential-time behaviour of rebar in 20, 30 and 40 MPa concrete

As per ASTM C-876 [36], −270 mV vs. SCE has been taken as threshold potential to reach active condition of rebar and this is included in the figures.

In 20 MPa concrete (Fig. 3), the rebar embedded in OPC concrete shows an initial potential value of −208 mV and it tends to become more negative with time. It attains more negative potential of −550 mV at the end of 200 days. In the case of PPC concrete, it shows −148 mV initially and it reaches more active potential of −464 mV at the end of 200 days. In the case of PSC concrete, the initial value is −151 mV and it reaches −415 mV at the end of 200 days. At the end of 824 days , the potential value is −438, −412 and −308 mV in OPC, PPC and PSC concrete, respectively.

In 30 MPa concrete (Fig. 4), OPC concrete shows an initial potential of −194 mV and attains more active potential of −564 mV at the end of 199 days. In the remaining exposure period it shows the potential more negative than −450 mV. In the case of PPC concrete, the initial value is −166 mV and reaches a more negative potential of −424 mV at the end of 199 days. But with exposure, the potential value shifted to −350 mV at the end of exposure. In PSC concrete, the initial value is −203 mV and attains more active potential of −478 mV at the end of 199 days. The potential shifted to a passive potential of −257 mV at the end of the exposure. Similar observation was reported [37] in field exposed concrete specimens of fly ash added concrete. It was stated that the initial potential value was −220 mV vs. CSE and after 18 months of exposure, the final value was −110 mV. Mohammed et al. [38] reported similar observation in slag added concrete, which showed more negative potential initially but has lesser corrosion rate at the end of the exposure.

It can be seen from Fig. 5, that the rebar in 40 MPa-OPC concrete is −195 mV initially and reaches a more active potential of −540 mV at the end of 824 days. In the case of PPC concrete, the initial value is −160 mV but attains active potential of −488 mV at the end of 147 days. With exposure the potential shifted to less negative potential of −325 mV at the end of 824 days. Whereas in the case of PSC concrete, though the rebar attains a maximum negative potential of −395 at the end of 121 days and it shifts less negative potential of −320 mV at the end of 824 days.

3.2. Macro cell corrosion current vs. time

In this galvanic current measurements, the +ve sign indicates the anodic current (corrosion current) and −ve sign indicates the cathodic current (passive current).

In 20 MPa concrete (Fig. 6), with time the macro cell current increases and shows maximum anodic current of 130 μA at the end of 308 days and after that the current decreases to a value of 50 μA at the end of 824 days of exposure. The initial increase in current value indicates the initiation and propagation of the corrosion process and after 300 days, the corrosion product formed on the rebar surface may retard the flow of corrosion current and this may reduce the current. In PPC concrete, the anodic current increases with time and reaches a maximum value of 46 μA at the end of 274 days and reduces to 6 μA at the end of the exposure. In the case of PSC concrete up to the period of 274 days, the rebar measures an anodic current of 18 μA and this reduces to a cathodic current of 12 μA at the end of the exposure.

The rebar in 30 MPa-OPC concrete is in passive condition which is indicated by the measured cathodic current up to 121 days then it increases to an anodic current of 38 μA at the end of 147 days (Fig. 7). At the end of exposure it reaches to a maximum current of 78 μA. The rebar in PPC concrete measures only cathodic current up to 231 days and increases to maximum anodic current of 6 μA at the end of 824 days. In the case of PSC concrete, initially up to 87 days the rod measures only cathodic current and shows an anodic current of 31 μA at the end of 308 days. After that it reduces to a cathodic current of 1 μA at the end of 824 days. The amount of chloride and moisture available at the time of measurement shifts the current both in anodic and cathodic direction during the exposure.

In 40 MPa concrete (Fig. 8) the rebar in OPC shows a maximum anodic current of 51 μA at the end of 537 days. In PPC concrete, the rebar shows maximum anodic current of 24 μA at the end of 308 days and after that the current reduces and it reaches a cathodic current of 11 μA at the end of 824 days. Similarly the rebar in PSC concrete initially measures an anodic current of 11 μA and then it reaches to 13 μA at the end of 308 days. Remaining exposure period it measures only cathodic current and reaches to 11 μA at the end of 824 days.

3.3. Visual observation

By comparing Figs. 9–11, the extent of rust is more on the rebar embedded in 20 MPa concrete than in 30 and 40 MPa concrete. In addition to this, the rebar in 20 MPa-OPC concrete is severely rusted throughout its length in all the four specimens whereas in PPC and PSC concretes corrosion observed only half the length of the rebar exposed in one specimen only whereas very negligible corrosion was observed on the rebar in another specimen. In 30 MPa concrete, the rebar in OPC concrete rusted severely throughout the length exposed whereas very negligible rusting is observed in PPC and PSC concrete. Similarly in 40 MPa concrete, only less than half the length of the rebar exposed corroded in OPC concrete whereas negligible corrosion was observed in PPC and PSC concrete.

3.4. Corrosion rate

Fig. 12 compares the corrosion rate of rebar in 20, 30 and 40 MPa concrete. This figure indicates that the rebar

in OPC concrete shows higher corrosion rate than in blended cement concretes among all the three concretes studied. In 20 MPa concrete. the corrosion rate is 0.0834, 0.0093, 0.0080 mmpy in OPC, PPC and PSC concrete, respectively. This indicates the rebar in PPC and PSC concrete has 9–10 times more corrosion resistance than OPC concrete ; In 30 MPa concrete, the corrosion rate is 0.0307, 0.0018, 0.0053 mmpy in OPC, PPC and PSC concrete respectively and shows that the rebar in PPC and PSC has 17, 6 times more corrosion resistance than OPC concrete, respectively. In 40 MPa concrete, the corrosion rate is 0.0095, 0.0058 and 0.0038 mmpy in OPC, PPC and PSC concrete, respectively, and indicates that the rebar in PPC and PSC concrete has 1.6, 2.5 times more corrosion resistance than OPC concrete respectively. The above corrosion rate values were very well correlated with the value measured in potential and macro cell corrosion current measurements.

3.5. Cl^- and OH^- ions in OPC concrete vs. blended cement concretes

3.5.1. Cl^- ions concentration

The concentration of chloride ions present in the blended cement concretes are invariably less than the OPC concrete at all depths studied except at 0–30 mm depth in 20 MPa concrete (Table 4). In 20 MPa concrete at 0–30 mm depth, the concentration of chloride ions in PSC concrete is 1.2 times less than the OPC concrete but in PPC concrete it is more than OPC concrete. The corrosion current and corrosion rate is less than the OPC concrete and this indicates that the core sample taken at that location may contain more amount of chlorides than the other portions. In other depths the chloride ion in blended cement concretes is 1.4–2.38 times less than the OPC concrete. Presence of lesser amount of chloride reduces the corrosion rate of rebar in these concretes. The concentration of chloride decreases with the increase of the depth. In 30 and 40 MPa concrete, the reduction of chloride ions in blended cement concretes is 1.4–3.1 times less than the OPC concrete in all depths studied. In 40 MPa concrete, in spite of higher chloride concentration at 0–30 mm depth lesser corrosion is observed on the rebar (Fig. 11). Because of higher cement content it has higher chloride threshold value for initiation of corrosion and this reduces the rate of corrosion of rebar.

3.5.2. OH^- ions concentration

Table 4 also shows the marginal reduction of OH^- ion concentration in PPC and PSC concrete than in OPC concrete. As the rebar is at 30 mm cover depth and comparing the value at 30–60 mm depth, the OH^- concentration is 6–10 times less in PPC and PSC concrete than in 20 MPa-OPC concrete and it is 2 and 1.6 times less in 30 MPa and 40 MPa concrete, respectively. Leaching of OH^- ions causes more reduction in alkalinity at 0–30 mm depth than at 30–60 mm and 60–90 mm depth. Higher cement content in 30 and 40 MPa – PPC and PSC concrete causes significant increase in OH^- ion concentration than in 20 MPa concrete.

3.6. Comparison of diffusion coefficient of chloride (D_a)

Fig. 13 compares the apparent chloride diffusion coefficient (D_a) of OPC concrete with PPC and PSC concretes. In 20 MPa concrete the D_a value is 5.575, 5.05 and 4.5×10^{-8} cm^2/s in OPC, PPC and PSC concrete, respectively. This shows in 20 MPa concrete not much reduction is observed between the OPC and blended cement concretes. But comparing the values in 30 and 40 MPa concrete significant reduction is observed. The D_a value is 1.6 times more in OPC concrete than the PPC and PSC concrete. The D_a value in 20,30 and 40 MPa-OPC concretes is varied from 5.525 to 5.975 and not much difference is observed between them. But in blended cement concretes the D_a value of 30 and 40 MPa concrete is 1.3 times less than the D_a value of 20 MPa concrete.

4. Discussions

For simulating marine substructure condition, the macro cell corrosion was created by varying the chloride ion concentration from top to bottom of the specimen. Thus the corrosion was accelerated by forming macro galvanic cell between top and bottom rebars and the distance between them was 15 cm. Hence the rate of corrosion is governed by the co-existence of both macro and micro galvanic cells on the rebar.

4.1. Potential vs. time

In 20 MPa concrete, the rebar in both OPC and blended cement concretes reached the more active potential at the end of 25 days than the threshold potential as specified in ASTM C876 and continuously remains in the active condition throughout the exposure period. The values indicated that the rebar in OPC concrete is in more corroding condition than in PPC and PSC concretes. Because of high porosity, more amount of chloride permeated and caused corrosion of rebar in all the three concretes. In 30 MPa concrete, comparatively the rebar in OPC and PPC concrete is in corroding condition whereas the rebar in PSC concrete is in passive condition. In 40 MPa concrete, the rebar in PPC and PSC concrete showed a value of −157 mV less negative than in OPC concrete. Hence it is inferred that in 40 MPa concrete also the rebar in OPC concrete is under more corroding condition than the rebar in blended cement concretes. Higher cement content and lower w/c ratio in 30 and 40 MPa concrete reduces the porosity of concrete. Reduction of porosity causes the reduction in the amount of chloride permeation during the exposure. In addition to this, presence of alumina in PPC and PSC concrete binds more amount of chloride.

Because of lesser chloride permeation and higher chloride binding ability the potential of rebar in blended cement concrete shifts less negative than the initial during the exposure.

4.2. Macrocell corrosion current vs. time

In 20 MPa concrete, the reduction of permeation of chloride and water causes the reduction of current for the rebar embedded in blended cement concretes. Formation of additional calcium hydrates by pozzolanic reaction [39] in PPC and PSC concrete, fills the pores in this highly permeable concrete and reduces the permeation of chloride and water [40]. The Al_2O_3 content of the PSC is more than that of PPC and OPC. This binds more amount of chloride and causes the rebar to measure cathodic current after 274 days. When comparing the anodic current at 147 days in 20, 30, 40 MPa-OPC concretes, it is 129 μA, 38 μA and 11 μA, respectively. This indicates that the magnitude of the current decreases with the increase of the strength of the concrete. Reduction of porosity in 30 and 40 MPa concrete because of lower w/c ratio and higher cement content causes the reduction of current in them when compared with the 20 MPa concrete. In the case of rebar in PPC and PSC concretes most of the period of exposure, the rebar measures only cathodic current and this indicates that the rebar is in passive condition in 30 and 40 MPa concrete. It is inferred that in 20 MPa concrete, the corrosion current of rebar is more than the rebar in 30 and 40 MPa concrete.

4.3. Corrosion rate

When compared with the OPC concrete, the reduction of corrosion rate by improved microstructure of blended cement concretes is more pronounced in 20 and 30 MPa concrete whereas this is not significant in 40 MPa concrete. In 40 MPa concrete because of dense pore structure it restricts the pore refinement by pozzolanic reaction in PPC and PSC concrete [39]. Whereas in 20 and 30 MPa concrete because of porous micro structure allow pore refinement to occur by pozzolanic reaction without any restriction.

4.4. Cl^- ion concentration

20 MPa concrete, being a high permeable the amount of chloride present at 0–30 mm depth is more than 7000 ppm and causes severe corrosion both in OPC and blended cement concretes. But in 30 and 40 MPa concrete, the chloride ions in PPC and PSC concrete is 1.6–2 times less than the OPC concrete. Thus the more amount of chloride present in 20 MPa concrete causes more corrosion current in 30 and 40 MPa concrete as shown in Figs. 9–11. The data confirms the formation of additional calcium hydrate fills the pores and causes the reduction of chloride penetration. This reduced chloride permeation causing the reduction of corrosion rate. In addition to this, the alumina content in the PPC and PSC concretes react with chloride and forms chloroaluminate causes the reduction of free chlorides in these concretes [41,42]. It was also reported [43] that C–S–H gel also binds chloride ions possibly in the interlayer spaces. Formation of additional C–S–H gels in blended cement concretes bind more amount of chlorides. Therefore both micro structural and chemical effects are the contributing factors for the reduction of chloride ions in PPC and PSC concretes.

4.5. OH^- ions concentration

Consumption of free calcium hydroxide ($Ca(OH)_2$) by pozzolanic reaction causes reduction of OH^- ions in PPC and PSC concrete. . This reduction of OH^- ion concentration is equal to the amount of fly ash/slag blended with cement and increased if the period of exposure is increased [44,16]. It is reported in 30% fly ash added concrete, the OH^- ion concentration of the pore solution is less than 70% of that of OPC concrete. Glass et al. [45] reported that the acid neutralization capacity of blended cement concretes is less than OPC. The reduction is 90%, 75% and 71% less than of OPC concrete in 20, 30 and 40 MPa concrete, respectively. The important inference is the reduction of alkalinity in blended cement concretes does not accelerate the corrosion of rebar even in presence of higher amount of chloride at the rebar level (30–60 mm). This longterm accelerated corrosion test concludes that in blended cement concrete, the minimum cement content shall not be less than 352 kg/m^3 for restoring the sufficient alkalinity to have higher chloride threshold value against rebar corrosion.

4.6. Diffusion coefficient of chloride (D_a)

The researchers reported that the chloride diffusion coefficient of normal strength concrete shall be varied from 1×10^{-8} cm^2/s to 1×10^{-10} cm^2/s [46–48]. The values obtained in all the concretes investigated lie between these values. It is also reported [41] after 2 years of marine exposure, in 40 MPa concrete the 'D_a' value was 5.56×10^{-8} cm^2/s and 2.75×10^{-8} cm^2/s for OPC and fly ash added concrete respectively. Similarly in the present investigation, after 847 days of exposure, the D_a value of 40 MPa concrete is 5.525×10^{-8} cm^2/s and 3.525×10^{-8} cm^2/s for OPC and PPC concrete, respectively.

It can be inferred that the interaction effect of higher chloride complexing ability and reduced chloride ion diffusivity by changes in physical structure of blended cement concretes enable them to perform better in terms of corrosion protection of reinforcing steel than the rebar in OPC concrete.

5. Conclusions

1. In 20 MPa concrete, corrosion rate of rebar in PPC and PSC concrete is 9 and 10 times less than the rebar in OPC concrete, respectively. In the case of 30 and 40 MPa concrete, it is 17, 6 and 1.6, 2.5 times less in PPC and PSC concretes than in OPC concrete, respectively.
2. Reduction of corrosion rate by improved microstructure of blended cement concretes is more pronounced in 20 and 30 MPa concrete whereas this is not significant in 40 MPa concrete when compared with OPC concrete.
3. The free chloride as observed in PPC and PSC concrete is less than the OPC concrete. Pore filling effect by pozzolanic reaction causes the reduction of chloride ion permeation in the former than the latter. In addition to this, the higher chloride binding ability of alumina present in the fly ash and slag causes the reduction of free chlorides in blended cement concretes.
4. Reduction of alkalinity in PPC and PSC concrete by 6-10 times when compared with OPC concrete does not affect the corrosion performance of rebar in blended cement concretes even in presence of higher amount of chlorides. But to have higher chloride threshold values against rebar corrosion the minimum cement content for blended cement concrete shall not be less than 352 kg/m^3.
5. Better performance of blended cement concrete in terms of corrosion rate and chloride ion permeation is attributed by the improved physical structure of concrete matrix characterized by reduced permeability of chloride and water.
6. Under this long term corrosion test in terms of durability, 40 MPa concrete which is having w/c ratio of 0.42 with cement content of 452 kg/m^3 performed better than the other two concretes.

References

[1] Sagues A. Detailed modeling of corrosion macrocells on steel reinforcing in concrete. Corros Sci 2001;43(12):1355–72.
[2] Rengaswamy NS, Balasubramaniyan TM, Srinivasan S, Mahadeva Iyer Y, Suresh Babu RH. Corrosion survey of bridges. Indian Concrete J 1987;42(3):147–60.
[3] Broomfield JP. Corrosion and residual life in concrete structures – an overview. Bull Electrochem 1995;11(3):121–8.
[4] Rendell F, Miller E. Macrocell corrosion of reinforcement in marine structures. In: Page CL, Treadway KWJ, Bamforth PB, editors. Corrosion of reinforcement in concrete. London: Elsevier Publishers; 1990. p. 167–77.
[5] Suzuki K, Ohno Y, Praparntanatorn S, Tamura H. Some phenomena of macro cell corrosion. In: Page CL, Treadway KWJ, Bamforth PB, editors. Corrosion of reinforcement in concrete. London: Elsevier Publishers; 1990. p. 87–95.
[6] Andrade C, Maribona IR, Feliu S, Gonzalez JA. The effect of macrocells between active and passive areas of steel reinforcements. Corros Sci 1991;33(2):237–49.
[7] Kahhaleh KZ, Carrasquillo RI, Wheat HG. Macrocell corrosion study of fabricated epoxy coated reinforcements. In: Swamy RN, editor. Corrosion and corrosion protection of steel in concrete, Sheffield. Sheffield Academic Press; 1994. p. 1244–53.
[8] Vedalakshmi R, Kumar K, Raju V, Rengaswamy NS. Effect of prior damage on the performance of cement based coatings on rebar: Macrocell corrosion studies. Cement Concrete Comp 2000;22:417–21.
[9] Sagues A. Performance of galvanized rebars in marine substructure service. Project ZE – 418; 1994; Part I, October.
[10] Broomfield JP. Assessing corrosion damage on reinforced concrete structures. In: Swamy RN, editor. Corrosion and corrosion protection of steel in concrete Sheffield. Sheffield Academic Press; 1994. p. 1–27.
[11] ASTM G109-94a. Standard test method for determining the effects of chemical admixtures on the corrosion of embedded steel reinforcement in concrete to chloride environment, ASTM Standards, 2000.
[12] Brown MC. Assessment of commercial inhibiting admixtures for reinforced concrete. Thesis (M.S.). Virginia Polytechnic Institute and State University; 1999.
[13] Bobrowski G, Youn DJ. Corrosion inhibition in cracked concrete: an admixture solution. In: Dhir RK, Jones HR, editor. Concrete 2000: Economic and durable construction through excellence, Proceedings of the international conference held at University of Dundee, UK, vol. 2. 7–9 September; 1993. p. 1249–61.
[14] Hussain SE, Rahseeduzzafar. Corrosion resistance performance of flyash cement concrete. ACI Mater J 1994;91(3):66–74.
[15] Ping Gu, Beaudoin JJ, Min-Hong Zhang, Malhotra VM. Performance of reinforcing steel in concrete containing silica fume and blast furnace slag ponded with sodium chloride solution. ACI Mater J 2000:254–62.
[16] Thomas M. Chloride thresholds in marine concrete. Cement Concrete Res 1996;26(4):513–9.
[17] Algahtani AS, Rasheeduzzafar, Alsaadoun SSI. Rebar corrosion and sulphate resistance of blast furnace slag cement. J Mater Civil Eng 1994;6(2):223–39.
[18] Detweiler RJ. Blended cements now and for the future. Rock Prod 1996:27–33.
[19] Baweja D, Harold Roper, Vute Sinivivatnanan. Chloride induced corrosion in concrete: Part I, corrosion rates, corrosion activity and attack areas. ACI Mater J 1998;95(3):207–17.
[20] Erhan Guneyisi, Turan Ozturan, Mehmet Gesoglu. A study on reinforcement corrosion and related properties of plain and blended cement concretes under different curing conditions. Cement Concrete Comp 2005;27:449–61.
[21] Macphee DE, Cao HT. Theoretical description of impact of blast furnace slag (BFS) on steel passivation in concrete. Mag Concrete Res 1993;45(162):63–9.
[22] IS 8112, Specification for 43 grade Ordinary Portland Cement, BIS Standards, New Delhi; 1989.
[23] IS 1489 (Part I): Specification for Portland Pozzolana Cement (fly ash based), BIS Standards, New Delhi; 1991.
[24] IS 455: Specification for Portland slag cement, BIS Standards, New Delhi; 1989.
[25] IS 1786: Specification for high strength deformed steel bars and wires for concrete reinforcement, BIS Standard, New Delhi; 1985.
[26] ASTM G 1-90, Standard Practice for preparing, cleaning and evaluating corrosion test specimens, ASTM Standards; 2000.
[27] Haque MN, Kayyali OA. Aspects of chloride ion determination in concrete. ACI Mater J 1995;92(5):532–41.
[28] Dhir RK, Jones MR, Ahmed HEH. Determination of total and soluble chlorides in concrete. Cement Concrete Res 1990;20:579–90.
[29] Kayyali QA, Haque MN. Environmental factor and concentration of Cl^- and OH^- in mortars. J Mater Civil Eng, Am Soc Civil Eng 1990;1(1):24–34.
[30] Dhir RK, Jones MR. Influence of PFA on proportion of free chlorides in salt contaminated concrete. In: Page CL, Treadaway KWJ, Bamforth PB, editors. Corrosion of reinforcement in concrete. Society of Chemical Industry; 1990. p. 227–35.

[31] Mangat PS, Molloy BT. Influence of flyash, slag and microsilica on chloride induced corrosion of reinforcement in concrete. Cement Concrete Res 1991;21(5):819–34.
[32] Muralidharan S, Vedalakshmi R, Saraswathy V, Palaniswamy N. Studies on the aspects of chloride ion determination in different types of concrete under macro cell corrosion condition. Build Environ 2005;40(9):1275–81.
[33] Berke S, Hicks MC. Predicting chloride profiles in concrete. Corrosion 1994;50:234–9.
[34] Browne RD. Mechanism of corrosion of steel in concrete in relation to design, inspection and repair of offshore and coastal structures. In: Performance of concrete in marine environment, Detroit, ACI SP – 65; 1980. p. 169–204.
[35] Abromowitz M, Stegan Irene A. In: Hand book of mathematical functions. New York: Royal Publications Inc.; 1970. p. 310–5.
[36] ASTM C 876 – 80 Standard test method for half-cell potentials of uncoated reinforcing steel in concrete, ASTM Standards; 2000.
[37] Sideris KK, and Savva AE. Resistance of fly ash and natural pozzolans blended cement mortars and concrete to carbonation, sulphate and chloride ion penetration. In: Proceedings 7th CANMET/ACI International conference on fly ash, silica fume, slag and natural pozzolans in concrete, vol. 1. SP-199, ACI, Detroit; 2001. p. 275–93.
[38] Mohammed TU, Toru Jamaji, Toshiyuki Ayoma. Marine durability of 15 year old concrete specimens made with ordinary Portland cement, slag, fly ash cements, in: Proceedings 7th CANMET/ACI International conference on fly ash , silica fume,slag and natural pozzolans in concrete, vol. 2. SP-199, ACT, Detroit; 2001. p. 541–60.
[39] Vedalakshmi R, Sundararaj A, Srinivasan S, Ganesh babu K. Quantification of hydrated cement products of blended cements in low and medium strength concrete using TG and DTA technique. Thermochem Acta 2003;407:49–60.
[40] Vedalakshmi R, Srinivasan S, Ganesh babu K. Studies on the strength and permeability characteristics of blended cements in low and medium strength concretes. Struct Concrete 2004;5(2):61–70.
[41] Thomas MDA, Mathews JD, Haynes CA. Chloride diffusion and reinforcement corrosion in marine exposed concretes containing pulverized fuel ash. In: Page CL, Treadaway KWJ, Bamforth PB, editors. Corrosion of reinforcement in concrete. Society of Chemical Industry; 1990. p. 198–212.
[42] Dhir RK, EI-Mohr MAK, Dyer TD. Chloride binding in GGBS concrete. Cement Concrete Res 1996;26(12):1767–73.
[43] Beaudoin JJ, Ramachandran VS, Feldman RF. Interaction of chloride and C–S–H. Cement Concrete Res 1990;20(6):875–83.
[44] Diamond S. Effect of two Danish fly ashes on alkali content of pore solutions of cement-fly ash pastes. Cement Concrete Res 1981;11(3):383–94.
[45] Glass GK, Reddy B, Buenfeld NR. Corrosion inhibition in concrete arising from its acid neutralization capacity. Corros Sci 2000;42(9):1587–98.
[46] Edogdu S, Kondratova IL, Bremner TW. Determination of Chloride diffusion co-efficient of concrete using open-circuit potential measurements. Cement Concrete Res 2004;34:603–9.
[47] Hobbs DW. Minimum requirements for durable concrete. Telford: British Cement Association; 1997. p. 135.
[48] Bader MA. Performance of concrete in coastal environment. Cement Concrete Comp 2003;25:539–48.